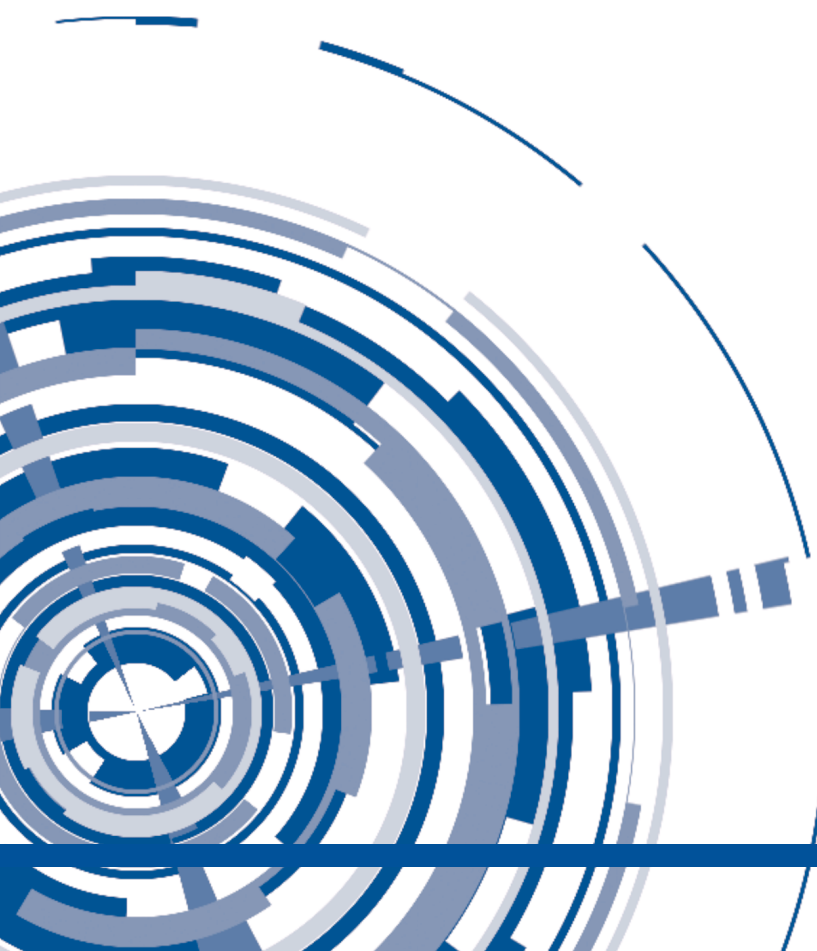


# ASME PTB-15-2023

## Full Matrix Capture Training Manual



PTB-15-2023

# FULL MATRIX CAPTURE TRAINING MANUAL



Date of Issuance: June 28, 2023

This publication was prepared by ASME Standards Technology, LLC (“ASME ST-LLC”) and sponsored by The American Society of Mechanical Engineers (“ASME”), Pressure Technology Codes & Standards.

Neither ASME, ASME ST-LLC, the authors, nor others involved in the preparation or review of this document, nor any of their respective employees, members or persons acting on their behalf, makes any warranty, express or implied, or assumes any legal liability or responsibility for the accuracy, completeness or usefulness of any information, apparatus, product or process disclosed, or represents that its use would not infringe upon privately owned rights.

Reference herein to any specific commercial product, process or service by trade name, trademark, manufacturer or otherwise does not necessarily constitute or imply its endorsement, recommendation or favoring by ASME or others involved in the preparation or review of this document, or any agency thereof. The views and opinions of the authors, contributors and reviewers of the document expressed herein do not necessarily reflect those of ASME or others involved in the preparation or review of this document, or any agency thereof.

ASME does not “approve,” “rate”, or “endorse” any item, construction, proprietary device, or activity.

ASME does not take any position with respect to the validity of any patent rights asserted in connection with any items mentioned in this document, and does not undertake to insure anyone utilizing a standard against liability for infringement of any applicable letters patent, nor assume any such liability. Users of a code or standard are expressly advised that determination of the validity of any such patent rights, and the risk of infringement of such rights, is entirely their own responsibility.

Participation by federal agency representative(s) or person(s) affiliated with industry is not to be interpreted as government or industry endorsement of this code or standard.

ASME is the registered trademark of The American Society of Mechanical Engineers.

No part of this document may be reproduced in any form,  
in an electronic retrieval system or otherwise,  
without the prior written permission of the publisher.

The American Society of Mechanical Engineers

Two Park Avenue, New York, NY 10016-5990

ISBN No. 978-0-7918-7623-7

Copyright © 2023

THE AMERICAN SOCIETY OF MECHANICAL ENGINEERS

All Rights Reserved

**TABLE OF CONTENTS**

Acknowledgements ..... xxii

Foreword ..... xxiii

1 HISTORY ..... 1

    1.1 ASME History..... 1

    1.2 ASME and FMC..... 3

    1.3 History of FMC and TFM ..... 5

    1.4 Equivalence of Early Developments ..... 6

2 FMC-TFM ..... 7

    2.1 Full Matrix Capture (FMC)..... 7

        2.1.1 Principle for Firing and Data Collection ..... 7

        2.1.2 FMC Signal Characteristics..... 7

        2.1.3 Typical FMC Signal Explained..... 8

        2.1.4 Alternative Firing and Data Collection Methods ..... 10

            2.1.4.1 Half Matrix Capture ..... 10

            2.1.4.2 Sparse Acquisition..... 11

        2.1.5 FMC Processes Using Different TR Methods..... 12

            2.1.5.1 Different Methods ..... 12

            2.1.5.2 Pulse Echo ..... 12

            2.1.5.3 FMC-TFM for Pitch/Catch..... 13

            2.1.5.4 Considerations..... 13

        2.1.6 FMC Data Size and Storage ..... 14

            2.1.6.1 The Full Data Set..... 14

            2.1.6.2 A-Scan Sample Count for Time Base Range ..... 14

            2.1.6.3 A-Scan Sample Size (Actual)..... 14

        2.1.7 FMC Data Storage..... 15

            2.1.7.1 Size ..... 15

    2.2 Total Focusing Method (TFM)..... 15

        2.2.1 TFM General ..... 15

        2.2.2 Principle for Data Reconstruction ..... 16

            2.2.2.1 B-Scan ..... 19

            2.2.2.2 A Note on TFM and Noise ..... 19

    2.3 Wave Type, Reconstruction Mode..... 20

        2.3.1 Naming Conventions..... 20

            2.3.1.1 Reconstruction Mode ..... 20

            2.3.1.2 Path..... 20

            2.3.1.3 Beam..... 20

            2.3.1.4 The Problem with Ray Tracing ..... 20

        2.3.2 TFM Modes..... 20

        2.3.3 Some Flaw Strategies ..... 22

        2.3.4 Beam Spread Considerations..... 22

        2.3.5 Self-Tandem Modes ..... 25

        2.3.6 Effects of Thickness ..... 26

    2.4 Amplitude Fidelity ..... 28

        2.4.1 Amplitude Fidelity in Signal Processing..... 28

        2.4.2 Grid Construction..... 30

        2.4.3 TFM Grid Resolution ..... 31

2.5	Scan Plan.....	34
2.5.1	Defining the Specimen and the Probe .....	36
2.5.2	Scan Plan for Specific Flaws.....	36
2.5.3	Locating the TFM Grid .....	37
2.5.4	Scan Plan Design.....	37
2.5.4.1	Volumetric Flaw (Void) in TT-TT Mode.....	37
2.5.4.2	Toe Crack in TT-TT Mode.....	38
2.5.4.3	Lack of Fusion T-T Mode .....	38
2.5.4.4	TT-TT Mode .....	39
2.5.4.5	Incomplete Penetration in T-T .....	39
2.5.4.6	Conclusion.....	39
2.6	Fourier and Hilbert Transforms.....	40
2.6.1	Time vs. Frequency Representation of Signals (Fourier Transform).....	40
2.6.1.1	Frequency representation of signals .....	40
2.6.1.2	Frequency Representation of A-scan .....	42
2.6.1.3	Examples in NDT.....	42
2.6.1.4	Example #1: Signal Filtering.....	42
2.6.1.5	Example #2: Probe bandwidth checking .....	44
2.6.2	Hilbert Transform.....	45
2.6.2.1	What is a Hilbert Transform?.....	45
2.6.2.2	How Can Hilbert Transform be Used in NDT?.....	45
2.6.2.3	What is the Envelope of a Signal?.....	45
2.6.2.4	Why Represent an A-Scan Signal with its Envelope Rather Than in an RF Form? ..	45
2.6.2.5	Conclusions .....	49
2.6.2.6	The Hilbert Transform is a Mathematical Function .....	49
2.6.2.7	Where the Hilbert Transform May Be Used .....	50
2.6.2.8	How the Hilbert Transform Can Be Used to Extract the Envelope of a Signal .....	52
2.6.2.9	How the Hilbert Transform Can Be Used for TFM Reconstruction .....	53
2.6.2.10	Computing a Hilbert Transform.....	53
3	TFMs.....	56
3.1	Synthetic Aperture Focusing Technique .....	56
3.1.1	Data Collection.....	56
3.1.2	Post Processing.....	57
3.1.3	Resolution.....	58
3.2	Virtual Source Aperture .....	59
3.3	Migration and Inverse Wave Extrapolation (IWEX), crossover between NDT and Geophysics .....	60
3.3.1	History of Migration in Geophysics.....	60
3.3.2	Examples of crossover between geophysics and NDT.....	61
3.3.3	Difference Between Basic FMC-TFM and IWEX.....	62
3.3.4	Data Displays Used for IWEX .....	62
3.3.5	Electronics Hardware .....	65
3.4	Iterative TFM .....	65
3.5	Adaptive TFM—A Framework.....	68
3.5.1	Basic Process.....	68
3.5.2	Metallurgical Study .....	69
3.5.3	Material Anisotropy Distribution Model.....	69
3.5.4	Material Properties and Wave Propagation in an Elastic Media.....	70
3.5.5	Cauchy Tensor, Christoffel Matrix, and Key Velocity Parameters.....	71

3.5.6	The Slowness Surface, Slowness Curves .....	71
3.5.7	Group velocity and Phase velocity .....	72
3.5.8	Detection of Anisotropic Characteristics.....	73
3.5.9	Path Dependent Adaptation Process.....	74
3.5.10	Model Evolution.....	75
3.5.11	Degrees of Freedom .....	75
3.5.12	TFM Process .....	76
3.6	PWI-ML .....	76
3.6.1	Plane Wave Imaging .....	76
3.7	Sectorial Total Focusing.....	78
3.7.1	STF, LTF, CTF Processes (Techniques but not Methods).....	78
3.8	TFMi™.....	80
3.8.1	Terminology .....	80
3.8.2	FMC Acquisition Characteristics .....	81
3.8.3	Propagation Modes.....	84
3.8.4	Region of Interest .....	84
3.8.5	Image Sensitivity.....	86
3.8.6	TFMi.....	86
3.8.7	Advantages of TFMi .....	88
3.9	Phase Coherence Imaging .....	88
3.9.1	What is PCI?.....	89
3.9.2	Interpreting PCI data .....	91
3.9.3	Conclusion.....	92
4	INSTRUMENTS .....	93
4.1	Hardware Challenges .....	93
4.1.1	The Challenge Posed by FMC.....	93
4.1.2	TFM Image Data Rate.....	93
4.1.3	The TFM Calculation Challenge .....	93
4.1.4	FPGA Performance .....	94
4.1.5	GPU Performance .....	94
4.1.6	FPGA/GPU Comparison .....	95
4.1.7	Adaptive and Iterative TFM.....	96
4.2	Deployment Schemes/Scanning Equipment.....	97
4.2.1	Introduction .....	97
4.2.2	Manual Scanning.....	97
4.2.3	Nonautomated Scanner.....	97
4.2.4	Semi-automated Scanner.....	98
4.2.5	Fully Automated Scanner.....	99
4.2.6	Application Specific .....	100
4.2.7	Conclusion.....	101
5	ARRAYS .....	102
5.1	Abstract .....	102
5.2	Basic Overview of Ultrasonic Transducers and Their Construction.....	102
5.2.1	What is a Transducer? .....	102
5.2.2	The Piezoelectric Effect .....	102
5.2.3	Types of Transducers .....	103
5.2.4	Basic Construction .....	104
5.2.5	Piezocomposite.....	106
5.3	Transducer Arrays .....	107

5.3.1	Linear Arrays.....	107
5.3.2	Construction of Transducer Arrays .....	108
5.3.3	Matrix Arrays .....	109
5.3.4	Common Configurations of Arrays Used in NDE .....	111
5.4	Transducer Sound Fields.....	113
5.4.1	Basic Beam Modeling.....	113
5.4.2	Near Field Distance.....	114
5.4.3	Focusing Flat and Curved Oscillators, Spot Size and Depth of Field.....	115
5.4.4	Beam Divergence/Array Element Performance .....	117
5.5	Array Design for FMC .....	119
5.5.1	Goal of FMC/TFM Imaging.....	119
5.5.2	Near Field Imaging.....	120
5.5.3	Angle Limitation/Constant Focal Ratio (F/D).....	121
5.5.4	Selection of Array Parameters (Active Plane).....	124
5.5.4.1	Frequency .....	124
5.5.4.2	Pitch/System Channels.....	125
5.5.4.3	Algorithms for Setting Active and Passive Plane Parameters.....	126
5.5.4.4	Linear Imaging FMC.....	126
5.5.4.5	Sectorial Imaging FMC.....	127
5.5.5	Strategy for Setting Passive Plane Parameters .....	128
5.5.6	Flat or Focused? .....	130
5.6	Transducer Standards .....	131
5.7	Conclusions and Recommendations.....	131
6	MODELING .....	132
6.1	General benefits of weld simulation.....	132
6.1.1	Effects of Material on Inspection Results .....	132
6.1.2	Better Understanding of Results via Simulation .....	134
6.2	Inspection Simulation.....	136
6.3	Using Modeling for TFM Inspection .....	140
6.3.1	Probe Selection.....	140
6.3.2	Mode of Propagation Selection.....	141
6.3.3	Modeling as TFM Scan Plan Assistance Tool .....	143
6.3.4	Example of Modeling as TFM Scan Plan Assistance Tool on ERW pipe .....	143
7	ADVANTAGES AND LIMITATIONS OF FMC/TFM VERSUS PAUT .....	147
7.1	Advantages .....	147
7.1.1	Accurate Visualization.....	147
7.1.2	Improved Resolution .....	149
7.1.3	Sound Propagation (dead zone).....	150
7.1.4	Near Surface Resolution.....	152
7.2	Limitations .....	152
7.2.1	Selection of the Correct Mode of Propagation for the Type of Flaws .....	152
7.2.2	Part Geometry and Material Definition.....	153
7.2.3	Attenuation and Penetration in Thick or Difficult to Penetrate Materials.....	153
7.2.4	Productivity .....	154
8	SIZING TECHNIQUES .....	155
8.1	Length and Height Sizing.....	155
8.1.1	Length Sizing .....	156
8.1.1.1	6dB Drop Length Sizing.....	156

8.1.1.2	6dB Drop Length Sizing Errors.....	158
8.1.2	dB Drop Through-Wall Height Sizing of Embedded Flaws .....	159
8.1.3	Tip Diffraction for Embedded Indications .....	161
8.1.4	Sizing Cluster Indications Such as Porosity.....	161
8.1.5	Tip Diffraction for Through-Wall Sizing of ID/OD-connected Cracks.....	162
8.1.6	Length and Height Sizing Comparisons with Various Methods–TFM, TOFD, PAUT 164	
9	FRACTURE MECHANICS FLAW CHARACTERIZATION.....	171
9.1	Introduction to Fracture Behavior .....	171
9.2	Overview of Fracture Mechanics .....	172
9.3	History of Fracture Mechanics .....	173
9.4	Two Main Categories of Fracture Mechanics .....	174
9.4.1	Summary .....	176
9.5	Application of Fracture Mechanics .....	176
9.5.1	Damage Tolerant Design.....	177
9.5.2	Planning for Inspection Using These Damage Tolerance Principles .....	178
9.6	ASME Code Margins and Safety .....	180
9.7	Flaw Evaluation Procedures Using Fracture Mechanics.....	180
9.7.1	Steps in the ASME BPVC Section XI Flaw Evaluation Procedure .....	181
9.8	Acceptance Criteria Examples .....	183
9.9	Applying the Acceptance Criteria Tables and Using Interpolation.....	187
9.9.1	Linear Interpolation.....	189
10	APPLICATIONS .....	193
10.1	In-service Inspections: FMC Techniques for High Temperature Hydrogen Attack Assessment.....	193
10.1.1	Problem Definition .....	193
10.1.2	Solution .....	194
10.1.3	Array Probes Design and Optimization.....	194
10.1.4	FMC Capabilities Validation.....	199
10.1.4.1	Samples Selection and Preparation .....	199
10.1.4.2	Experimental Setups.....	200
10.1.4.3	Distance Calibration.....	200
10.1.4.4	Amplitude Fidelity .....	201
10.1.4.5	Sensitivity and Resolution.....	202
10.1.4.6	Investigation of Samples with Machined Flaw .....	204
10.1.4.7	Investigation of Samples with Synthetic HTHA Damage.....	207
10.1.4.8	Investigation of Samples Removed from Service (Progressive Validation) .....	211
10.1.5	Conclusions .....	226
10.2	FMC/TFM Based Inspection of Small-Diameter Components for FAC Damage.....	226
10.2.1	Summary .....	226
10.2.2	Background .....	226
10.2.3	Feeder Pipes .....	227
10.2.4	Degradation Mechanism.....	227
10.2.5	Component Description.....	228
10.2.6	Inspection Specification Requirements .....	229
10.2.7	Complicating Factors .....	230
10.2.8	Overview .....	232
10.2.9	Separation of Tasks .....	232



10.2.10 Training .....	232
10.2.11 Equipment .....	233
10.2.12 Software .....	234
10.2.13 Calibration.....	234
10.2.14 Data Acquisition Process.....	235
10.2.15 Recording .....	236
10.2.16 Data Acquisition Procedure.....	236
10.2.17 Data Analysis Process .....	238
10.2.18 Data Analysis Procedure .....	241
10.2.19 Results .....	241
10.2.20 Discussion .....	243
10.2.21 Further Developments .....	246
10.2.22 Conclusions .....	246
10.3 Crack Growth Monitoring with PAUT and TFM.....	247
10.3.1 Introduction .....	247
10.3.2 Approach .....	247
10.3.3 Description of the UT Setup.....	249
10.3.4 Results .....	250
10.3.5 Analysis.....	250
10.3.6 Conclusions and Next Steps.....	256
10.4 Weld Examination-Introduction .....	257
10.4.1.1Procedures .....	257
10.4.2 Equipment .....	258
10.4.2.1Instruments .....	258
10.4.2.2Probes .....	258
10.4.2.3Wedges .....	258
10.4.3 Getting Started.....	258
10.4.4 Scan Plan.....	259
10.4.4.1Search units .....	260
10.4.4.2Image Paths .....	260
10.4.5 Equipment Set-Up .....	261
10.4.5.1Image Grid Density .....	261
10.4.5.2TFM Frame Size.....	262
10.4.5.3Grouping.....	262
10.4.6 Scanning/Data Collection.....	263
10.4.6.1Encoding.....	264
10.4.6.2Weld Examination Scan Strategy.....	265
10.4.6.3Artifacts.....	265
10.4.7 Evaluation.....	266
10.4.7.1Data Views .....	266
10.4.7.2Detection .....	267
10.4.7.3Characterization .....	267
10.4.8 Examples .....	269
References .....	275
Appendix A: FMC-TFM Data of Internal Surface (ID), External Surface (OD) and Mid-Wall Types of Defects Represented by Notches .....	278
Appendix B: TFM Data Presentation and Flaws Sizing.....	303

**LIST OF FIGURES AND TABLES**

Figure 1-1: Period Repair Work on a Riveted Seam ..... 1

Figure 1-2: The Steamship Sultana ..... 2

Library of Congress, Prints & Photographs Division, Civil War Photographs, LC-DIG-ppmsca-34001 ..... 2

Figure 1-3: Policeman Next to Another Failed Boiler ..... 2

Figure 1-4: The Before and After of the Grover Shoe Factory in Brockton, Massachusetts ..... 3

Figure 1-5: Static Screen Shot from the Applus IWEX System..... 4

Figure 2-1: Firing Pattern and Resulting Matrix for FMC ..... 7

Table 2-1: Breakdown of the FMC signal data as represented on images ..... 8

Figure 2-2: Example of Redundant Pairs ..... 10

Figure 2-3: Firing Pattern and Resulting Matrix for HMC ..... 11

Figure 2-4: Firing Pattern and Resulting Sparse Acquisition of 1:2, 1:4, and 1:8 ..... 11

Figure 2-5: Example of a Possible SMC with 1:2 Sparsity ..... 12

Figure 2-6: Schematic of a Side-by-Side Pitch Catch Configuration..... 13

Figure 2-7: Wave Propagation Path for a Transmit-Receive Pair to a Specific Pixel..... 16

Figure 2-8: TFM being constructed from a single transmit and receive pair. Note that as it progresses, each individual pixel has a set of delays and an intensity reported for its location. .... 17

Figure 2-9: The Cumulative TFM (lower right) becomes a compilation of all T&R pairs. This example is only four T&R pairs. .... 18

Figure 2-10: We have progressed from the previous cumulative TFM of 4 pairs to 410 pairs (left) or about 10% complete. For this component, a set of side drilled holes have formed. In the image to the right, which is 2,048 pairs or about 50% complete, you can further see the effects of the summation process by witnessing that the large “swath” of noise in the image has begun to clear up. .... 18

Figure 2-11: The final image at 100% (all 4,096 pairs) completed. It is important to consider the order of magnitude with which we have progressed through these images. We started with a single pair assigning data to every pixel, then went to 4 pairs, then 410 pairs, then 2,048, then finished at 4,096 pairs. (1) ..... 19

Figure 2-12: Example of How Mode Nomenclature Works. .... 21

Figure 2-13: Schematic of Some Common Reconstruction Modes ..... 21

Figure 2-14: Examples illustrating the advantages of different reconstruction modes in detection of certain flaws ..... 22

Figure 2-15: (a) and (b) Position of the pixel in the TFM frame; (c) and (d) acoustic field simulation using the function of beam spread dedicated to the pixels in (a) and (b), respectively..... 23

Figure 2-16: Coverage that can be obtained with (a) standard phased array sectorial sweep and (b) TFM in TT-TT mode..... 24

Figure 2-17: Valid location for a TFM frame reconstructed using T-T and TT-TT modes ..... 24

Figure 2-18: Inappropriate TFM frame location for TT-TT reconstruction mode ..... 25

Figure 2-19: Inappropriate TFM frame location for T-T reconstruction mode ..... 25

Figure 2-20: Examples of the Expected Response from Self-tandem Modes ..... 26

Figure 2-21: An example illustrating the inefficient spatial coherence of the TFM trajectories for a specimen with different thickness than the nominal value used for image reconstruction. In a.) the actual and input thickness is the same, in b.) the actual thickness is less than the input thickness, in c.) the actual thickness is greater than the input thickness. The delays remain the same..... 26

Figure 2-22: Maps of the amplitude envelope computed using the TFM on the three samples of different thicknesses, using: (a) 20 mm (nominal), (b) 18 mm, (-10%), and (c) 22 mm (+10%) wall thickness samples. (Courtesy of Olympus NDT Canada INC.) [Painchaud-

April, G., Badeau, N. and Lepage, B., 2018, April. Total focusing method (TFM) robustness to material deviations. In AIP Conference Proceedings (Vol. 1949, No. 1, p. 200007). AIP Publishing LLC.] ..... 27

Figure 2-23: The dependency that the self-tandem modes, T-TT, and TT-TTT, in this case, rely upon having an accurate thickness value for the delay calculation ..... 28

Figure 2-24: Inaccuracy in signal digitalization and Amplitude Fidelity for signal digitized at a frequency of 5 points per wavelength..... 29

Figure 2-25: Inaccuracy in signal digitization and Amplitude Fidelity for signal digitized at a frequency of 2 points per wavelength..... 29

Figure 2-26: Principal parameters of a TFM frame..... 30

Figure 2-27: (a) Signal amplitude distribution on the lateral axis as a result on the interaction between the beam at its minimum waist with a point scatterer and (b) Representation of the (rectified) amplitude TFM image of a hypothetical point scatterer using a common large bandwidth pulsed signal spanning  $1.5\lambda$  in length. The minimal structure to sample in amplitude is the  $\lambda/2$  oscillation [TFM Grid Resolution by Olympus Scientific Solutions Americas] ..... 32

Figure 2-28: Impact of the pixel size of the TFM image on the reliability and fidelity of TFM results ..... 33

Figure 2-29: Impact of pixel size used for TFM image reconstruction on the signal amplitude of an SDH. The signal amplitude changes with the TFM pixel size from (a) 87.1% FSH for  $\lambda/6$ , to (b) 42.6% FSH for  $\lambda/3$ , and finally to (c) 8.7% FSH for  $\lambda$ ..... 34

Figure 2-30: A schematic of the parameters required to define the region of interest in TFM configuration ..... 35

Figure 2-31: Schematic of the welded joint specimen for scenarios A and B..... 36

Figure 2-32: Acoustic paths and corresponding reconstruction modes for optimal detection of under evaluation flaws..... 36

Figure 2-33: Different TFM modes required to extend the coverage..... 37

Figure 2-34: Schematic of the applied grid ..... 37

Figure 2-35: (a) Simulated acoustic field and (b) ray tracing results for a void located in the weld material..... 37

Figure 2-36: (a) Simulated acoustic field and (b) ray tracing results for a toe crack ..... 38

Figure 2-37: (a) Simulated acoustic field and (b) ray tracing results for a toe crack using T-T..... 38

Figure 2-38: (a) Simulated acoustic field and (b) ray tracing results for a toe crack using TT-TT..... 39

Figure 2-39: (a) Simulated acoustic field and (b) ray tracing results for an incomplete penetration ... 39

Figure 2-40: Examples of time signals: (a) A-scan, (b) electrocardiogram (ECG)–(c) piece of music ..... 40

Figure 2-41: Time (b) and frequency (c) representation of a piece of music signal (a) ..... 41

Figure 2-42: Time (a) and frequency (b) representation of an A-scan ..... 42

Figure 2-43: Workflow of a filtering process in the frequency domain: Fourier transform of the noisy signal (a)–Multiplication of the spectrum with the transfer function of the filter (b)–Inverse Fourier transform of the filtered spectrum (c)..... 43

Figure 2-44: Time representation of a noisy A-Scan (a) and a filtered A-Scan (b). In this example the SNR of the filtered signal  $x'(t)$  is 6 dB higher than the SNR of the noisy signal  $x(t)$ .. 43

Figure 2-46: Temporal A-Scan (a) and its spectrum (absolute value of the Fourier transform obtained thanks to a FFT and for positive frequencies only) (b)..... 44

Figure 2-47: FFT feature on the Olympus-MX2 ..... 44

Figure 2-48: Example of a zero-mean A-scan (blue) and its envelope (red)..... 45

Figure 2-49: (a) Rectified signal (A-scan) (blue) and estimated envelope of the same A-scan (red)– (b) Details showing corresponding errors of both maximum amplitude and time position estimation of the maximum amplitude ..... 46

Figure 2-50: Example of TFM images of SDH: with rectified (absolute value) TFM (a)–with TFM envelope (b). Consequently, the occurrence of having several maxima is a challenge for estimating accurately the position of the maximum value of an indication within TFM images. This issue is illustrated in Figure 2-51. This point justifies having an interest in the construction of the envelope, in the specific case of TFM images..... 47

Figure 2-51: TFM images of a defect (SDH) showing a gap in the vertical position estimation of the maxima amplitude. (a) In-phase TFM–(b) Quadrature TFM–(c) Envelope TFM..... 47

Figure 2-52: Examples of an ID connected crack. TFM image on the left with envelope and on the right without envelope..... 48

Figure 2-53: Examples of a slag indication. TFM image on the left with envelope and on the right without envelope. .... 48

Figure 2-54: Transfer function of a Hilbert transform. (a) Modulus–(b) Phase ..... 50

Figure 2-55: Pure sine signal spectrum. (a) cosine—(b) sine..... 51

Figure 2-56: Detail of the In-phase signal  $x_1(t)$ (original A-scan, cf. Figure 2-42) (blue), quadrature component  $x_1(t)$  obtained thanks to a Hilbert transform (green), and the envelope  $A(t)$  (red). .... 52

Figure 2-57: Computation of the envelope TFM from two FMCs in quadrature..... 53

Figure 2-58: (a) Modulus of the In-phase signal spectrum – (b) filtering function – (c) Modulus of the analytical signal spectrum ..... 54

Figure 2-59: Example of an impulse response for a type III generalized linear phase discrete Hilbert transformer of order 20..... 55

Figure 2-60: Implementation of the TFM envelope computation (a) In the frequency domain–(b) In the time domain..... 55

Figure 3-1: Reproduced from NUREG CR 3625-Busse 1984 ..... 57

Figure 3-2: Reproduced from NUREG CR 3625–Busse 1984..... 57

Figure 3-3: Reproduced from NUREG CR 3625–Busse 1984..... 58

Figure 3-4: Reproduced from NUREG CR 3625–Busse 1984..... 59

Figure 3-5: Principle of VSA. Array elements are excited with a delay lay to produce the intended wavefront, as if coming from a virtual source..... 59

Figure 3-6: On the left, a seismic shot record. On the right, ultrasonic NDT data displayed in the way customary in seismic exploration..... 61

Figure 3-7: Part of Figure 4.8 from thesis Niels Pörtzgen, 2007..... 63

Figure 3-8: Example of an IWEX image combining multiple modes ..... 63

Figure 3-9: Example of a typical IWEX image showing expanded color scale..... 64

Figure 3-10: Example of multiple modes / views, including a 3D image ..... 64

Figure 3-11: Generic Imaging Process for Iterative TFM..... 66

Figure 3-12: An example of an edge detection process identifying leading and trailing edges of a TFM image. The image itself has been removed to enable view of the detected edges..... 67

Figure 3-13: Block diagram of a generic Adaptive TFM process. The diagram also shows inputs to the main portion of the adaptive loop..... 69

Figure 3-14: Framework for a distributed parameter model of a hypothetical configuration ..... 70

Figure 3-15: Cauchy tensor depicting tensile and shear vectors associated with a unit volume. Right–matrix representation of Cauchy tensor..... 71

Figure 3-16: Examples of phase slowness curves, left–isotropic materials where the velocity remains constant irrespective of direction, right–anisotropic where velocity varies with direction..... 72

Figure 3-17: Phase and Group velocity vectors plotted on a slowness curve. The magnitude of the change has been exaggerated for the purpose of illustration..... 73

Figure 3-18: Sample, left with normal beam A scan response center. Note the phases remain consistent in each multiple. .... 74

Figure 3-19: Sample, left, A scan response center. Note the phase of the initial response is the same as Figure 3-18, whereas the phase is changed in subsequent signals. This behavior is indicative of anisotropy. .... 74

Figure 3-20: Examples of solution condition ..... 75

Figure 3-21: Plane waves generated for three different angles ..... 76

Figure 3-22: comparison of FMC/TFM image (top right) to PWI image (bottom right) for PWI setup with 6 plane wave angles (left) ..... 77

Figure 3-23: Screen shot comparison of classic TFM vs PWI next to microetch from the component. .... 78

Figure 3-24: A comparison of TFM, STF, and standard PA ..... 79

Figure 3-25: A schematic of the (a) STF, (b) LTF, and (c) CTF sweep..... 79

Figure 3-26: FMC scanning sequence ..... 81

Figure 3-27: TFM beam summed to generate a pixel from the 1st to the 64th element..... 82

Figure 3-28: Data acquisition and the generation of TFM image for a specific pixel..... 83

Figure 3-29: TFM image generation principle ..... 83

Figure 3-30: Index setup..... 84

Figure 3-31: Depth setup..... 85

Figure 3-32: Resolution setup for index and depth ..... 85

Figure 3-33: Toe crack. TFMi image on the right (2T-3T-4T) and sectorial scan on the left..... 87

Figure 3-34: Sectorial scan, TFM images (2T-5T) and TFMi image for a sequence of side drilled holes vertically aligned..... 87

Figure 3-35: TFMi image on the left and side view of a sample with a crack ..... 88

Figure 3-36: DAS Algorithm (above), and DAS with Phase Information Applied Post Hilbert Transform (below)..... 89

Figure 3-37: Shows statistical approach with randomized process and the variance difference of coherence vs. non-coherence areas..... 89

Figure 3-38: Shows high variance in coherence and non-coherence areas for noise to indication discrimination..... 90

Figure 3-39: The entire hook crack can be seen with only the TT-TT group on the left in PCI, where two groups are needed with conventional TFM (TT-T and TT-TT) on the left. The crack can be sized using the tip diffraction. .... 91

Figure 3-40: Shows High Temperature Hydrogen Attack (HTHA) PCI data on the left, and conventional amplitude based TFM on the right..... 92

Figure 3-41: Shows Creep Damage PCI data on the left, and conventional amplitude based TFM on the right..... 92

Figure 4-1: Schematic architecture of an FPGA (top) vs and GPU (bottom) based system ..... 95

Figure 4-2: Timeline showing the progression of GPUs..... 96

Table 4-1: Comparative Chart of FPGA and GPU Processors..... 97

Figure 4-3: Examples of wheel type encoders..... 98

Figure 4-4: Some examples of Semi-automated (chain) scanners, and the use of a laser guided system (bottom right) ..... 99

Figure 4-5: Examples of a fully automated scanner ..... 100

Figure 4-6: Examples of an elbow scanner (left), and a paintbrush scanner (right)..... 101

Figure 5-1: Direct (a) and inverse (b) piezoelectric effect. The most common transduction mechanism used in ultrasonic transducers for industrial, medical, and commercial ultrasound applications. .... 103

Figure 5-2: Various types of ultrasonic transducers that can be found in industrial NDT, including (a) single element contact transducers, (b) bespoke transducer design for turbine disk inspection, and (c) high temperature, wedge mount linear arrays for weld inspection .... 103

Figure 5-3: Basic transducer constructional elements for industrial single (a) and dual (b) element piezoelectric transducers. .... 104

Figure 5-4: Schematic representation of piezocomposite material in a) 2-2 connectivity and b) 1-3 connectivity ..... 106

Figure 5-5: Schematic view of linear array geometry showing electronic control over a sub aperture of the array which allows electronic control of the beam (steering, focusing and scanning). Elevation performance is fixed by the frequency and aperture size and potential addition of a focusing lens..... 107

Figure 5-6: Basic constructional elements of the acoustic stack of a linear array. A complete transducer would additionally have a transducer case and micro-coaxial cable/connector assembly. .... 108

Figure 5-7: 840 element 1.5D array (420 electrical connections) showing cable assembly with four, 128 channel cable assemblies with IPEX connectors..... 109

Figure 5-8: 2D matrix array. The secondary axis of beam control allows electronic manipulation of the beam in three dimensions: azimuth, elevation, and depth at the expense of increased channel count and system complexity. .... 110

Figure 5-9: Taxonomy for matrix arrays showing the increased control over the elevation plane that can be achieved in tradeoff to increasing channel count and system complexity. .... 110

Figure 5-10: Common array geometries used in non-destructive testing applications..... 111

Figure 5-11: Field II/Matlab beam simulation from a 5MHz, 12.7mm diameter ultrasonic transducer radiating into water. Sound intensity is indicated by the color scale in relative units ..... 113

Figure 5-12: Modeled sound field of a flat ultrasonic transducer, showing the intensity fluctuations in the near field transitioning to a smoothly varying beam at and beyond the Near Field Distance,  $N$ . .... 114

Figure 5-13: -6dB spot size ( $E_x$ ) and -3dB depth of field ( $E_z$ ) for flat and focused circular transducers..... 116

Table 5-1: Approximate formulas for -6dB spot size for flat and focused oscillators, narrow band approximation..... 116

Figure 5-14: Graphical representation of valid, marginal, and invalid element contributions due to the limitations of element beam divergence ..... 117

Figure 5-15: Schematic representation of beam divergence half angle..... 118

Figure 5-16: One way (free field) and two way (pulse echo) response for an array element two wavelengths in size ( $D/\lambda=2$ )..... 118

Figure 5-17: -6dB divergence half angle for element size in wavelengths (pulse echo)..... 119

Figure 5-18: B-scan view of a  $\varnothing$  1 mm SDH Standard using a 5 MHz linear array, 64 elements, LW wedge: Standard phased array (right) compared to FMC/Sectorial Total Focusing (STF) method (center) and FMC/Total Focusing Method (TFM) (right). Note that for standard PA, the targets are only in focus at a single depth. .... 120

Figure 5-19: B-scan view of a  $\varnothing$  1 mm SDH Standard using a 5 MHz linear array, 64 elements, LW wedge with varying aperture size. Note the reduction in resolution that corresponds with decreasing aperture size with corresponding increase in the effective lateral beam size..... 120

Figure 5-20: Example of probe and wedge configuration with consequent near field area and the region of interest on 25mm thick carbon steel weld..... 121

Figure 5-21: Beam divergence plots for element sizes of a)  $0.5\lambda$  b)  $1.0\lambda$  and c)  $4.0$  ..... 122

Figure 5-22: CIVA simulations of direct-contact imaging, contrasting the results of TFM using 0.5, 1, and 1.5 wavelength elements, with and without angle limitation. (a)-(c) processed using a Conventional TFM algorithm, (d)-(f) processed with angle limits (cone filter) of 30, 30, and 19.5 degrees, respectively. Results obtained using the following arrays: (a), (d) 64 element/0.63mm pitch ( $0.5\lambda$ ), (b), (e) 32 element/1.26mm pitch ( $1\lambda$ ) and (c), (f) 21 element/1.89 mm ( $1.5\lambda$ ) pitch..... 123

Table 5-2: Computations of achievable resolution based on element size, beam divergence and resulting focal ratio and focusing effect. .... 123

Figure 5-23: Schematic representation of critical parameters for linear scanning and sectorial scanning FMC/TFM..... 125

Figure 5-24: Simulations of cross-sectional beam profile at focal point of flat and elevation focused linear arrays. Ideal “circular” beam profile has equal sizing capability in both the active and passive plane. More commonly, the beam profile is elliptical, having non-uniform sizing and resolution capability. .... 129

Figure 5-25: Simulations of varying beam spot size for flat and elevation focused linear arrays. The ultrasonic beam is only truly in focus when both the azimuth and elevation are focused. Variation in imaging performance will be seen due to the variation in elevation spot size for flaws that are smaller than the beam spot due to Area-Amplitude. .... 129

Figure 6-1: Coarse grain (left) compared to isotropic material (right) with L0 immersion ..... 132

Figure 6-2: Fields radiated by the 45 T-wave transducer in isotropic (left) and anisotropic (right) specimens ..... 132

Figure 6-3: Beam of phased array transducer focused on weld prep ..... 133

Figure 6-4: E=0.13mm ..... 133

Figure 6-5: E=0.26mm ..... 133

Figure 6-6: Mode Identification (Mode ID) ..... 134

Figure 6-7: Example of a modeling simulation using the immersion technique..... 134

Figure 6-8: 45-degree L wave is shown on the left and 45 degree T wave is shown on right ..... 135

Figure 6-9: Chart of flaw tilt vs. amplitude..... 135

Figure 6-10: B-scan 3D model for transverse 45 degree (T45) refracted angle interacting with from left to right: 0°, -5° and -10° flaw tilt ..... 136

Figure 6-11: Raw results of the FMC simulation..... 137

Figure 6-12: Comparison of 3D iso-surfaces (left column) and YZ section (right column) images after TFM reconstruction without (first row) and with (second row) 'envelope signal ' as the computation option..... 137

Figure 6-13: 3D view of inspection setup with backwall breaking planar flaw ..... 138

Figure 6-14: TT-T reconstruction..... 138

Figure 6-15: L-L reconstruction ..... 138

Figure 6-16: T-T reconstruction ..... 138

Figure 6-17: LL-L reconstruction..... 138

Figure 6-18: Inspection for Lack of Fusion 1 ..... 139

Figure 6-19: T-T wave type..... 139

Figure 6-20: TT-TT wave type..... 139

Figure 6-21: Far field directivity pattern of a 3mm pitch element in Rexolite at 5 MHz..... 141

Figure 6-22: TFM inspection of a root crack in T-T mode ..... 142

Figure 6-23: TFM inspection of a root crack in TT-T mode..... 142

Figure 6-24: a) Longitudinal scanner mounted on the ERW pipe sample, along with TFM flaw detector device showing the stacked vertical lack of fusions located inside the weld line. The flaws span about 25.4mm long over the pipe axis. b) Scan plan representing the weld and curvature of sample..... 144

Figure 6-25: The modeling for planar defect “heatmaps” computed for (a) the TT-T and (b) TT-TTT mode of propagations..... 145

Figure 6-26: TFM image on the stacked lack of fusion flaws for (a) the TT-T and (b) TT-TTT. The gain is adjusted to equalize the maximum amplitude..... 146

Figure 7-1: ID connected crack detection comparison between PAUT and TT-TT TFM ..... 147

Figure 7-2: OD connected crack detection comparison between PAUT and TT-TT TFM..... 148

Figure 7-3: ID connected crack detection comparison between PAUT and TT-T TFM..... 148

Figure 7-4: OD connected crack detection comparison between PAUT and TT-TTT TFM ..... 148

Figure 7-5: PAUT detection of SDH at different depths.....	149
Figure 7-6: TFM L-L mode detection of SDH at different depths.....	150
Figure 7-7: Detection of vertically stacked SDH comparison between PAUT and TFM L-L mode of propagation.....	151
Figure 7-8: Detection of link between blisters with TFM.....	151
Figure 7-9: Detection of shallow SDH comparison between PAUT and TFM L-L mode of propagation.....	152
Figure 7-10: Lack of fusion detection comparison between TFM TT-TT and TT-T modes .....	152
Figure 7-11: Vertical notch detection comparison with a TT-T mode of propagation: accurate velocity vs. 2.5% velocity input error.....	153
Figure 7-12: SNR difference at the detection of a flat bottom hole (FBH) between a 32 element Linear PAUT scan and TFM L-L mode.....	154
Figure 8-1: Measurement Tools–Cursors.....	155
Figure 8-2: Principles of 6dB Drop length sizing of discontinuities larger than the beam diameter .	156
Figure 8-3: Example of LOF 6dB Drop length sizing.....	157
Figure 8-4: Principles of 6dB Drop length sizing of discontinuities smaller than the beam diameter .....	157
Figure 8-5: Example of slag indication length using maximum amplitude sizing technique.....	158
Figure 8-6: Example of ID HAZ crack indication length using maximum amplitude sizing technique .....	159
Figure 8-7: Example of dB Drop Through-Wall Height Sizing technique .....	160
Figure 8-8: Through-Wall Height Sizing of LOF using Tip Diffraction technique.....	161
Figure 8-9: Through-Wall Height Sizing of Porosity cluster using Tip Diffraction technique.....	162
Figure 8-10: Through-Wall Height Sizing of cracks using Tip Diffraction technique: ID connected crack on 1 in. thick specimen. T-T image path. Red reference cursor on ID surface, green measurement cursor on deepest crack tip. D(m-r) reading of 0.485 in. shows through-wall height of crack. ....	163
Figure 8-11: Through-Wall Height Sizing of cracks using Tip Diffraction technique: OD connected crack on 1 in. thick specimen. TT-TT image path. Red reference cursor on OD surface, green measurement cursor on deepest crack tip. D(m-r) reading of 0.813 in. shows through-wall height of crack. ....	163
Figure 8-12: Weld Joint Geometry for 1 in. (25 mm) Samples.....	164
Figure 8-13: Flaw Sample Manufacturer’s Record of Sizing Tolerances .....	164
Table 8-1: A flaw sizing comparison between multiple methods .....	164
Figure 8-14: Images of Indication # 1–Lack of Sidewall Fusion: (a) TFM–T-T mode, (b) TOFD Non-Parallel Scan, (c) PAUT Sectorial Scan.....	165
Figure 8-15: Images of Indication # 2–ID Crack: (a) TFM-T-T mode, (b) TOFD Non-Parallel Scan, (c) PAUT Sectorial Scan .....	166
Figure 8-16: Images of Indication # 3 Porosity: (a) TFM T-T mode, (b) TOFD Non- Parallel Scan, (c) PAUT Sectorial Scan .....	167
Figure 8-17: Images of Indication # 4 Slag: (a) TFM T-T mode, (b) TOFD Non-Parallel Scan, (c) PAUT Sectorial Scan.....	168
Figure 8-18: TFM Images of OD-Connected Crack .....	169
Figure 8-19: TFM Images of ID-Connected Crack.....	169
Figure 8-20: TFM Images of Slag.....	170
Figure 8-21: TFM Images of LOF-Far Side Bevel-Height Sizing using Tip Signals .....	170
Figure 9-1: Load vs. Displacement from Testing of a Brittle and Ductile Material .....	171
Table 9-1: Strength of Materials vs Fracture Mechanics Method.....	172
Figure 9-2: The Three Elements Related to Component Fracture.....	172
Figure 9-3: Catastrophic Failure of a Liberty Ship During World War 2 .....	173
Figure 9-4: Pellini’s Fracture Analysis Diagram (FAD).....	174



Figure 9-5: The Two Types of Fracture Mechanics Methods ..... 175

Figure 9-6: The Three Modes of Cracking..... 175

Figure 9-7: Illustration of Analysis of Flaws as a Function of Time..... 177

Figure 9-8: Stepwise process for Damage Tolerant Design ..... 178

Figure 9-9: ISI Sequence ..... 182

Figure 9-10: Flaw Evaluation Procedure..... 183

Figure 9-11: From ASME B31.3-2022 ..... 184

Figure 9-12: From ASME BPVC Section VII-2021 ..... 185

Figure 9-13: From ASME BPVC Section XI-2021..... 187

Figure 9-14: Depiction of surface or subsurface flaw proximity rules from ASME B31.3-2022..... 188

Figure 9-15: The aspect ratio column in red..... 189

Figure 9-16: Example of When Interpolation May be Needed ..... 190

Figure 9-17: Interpolation Graph for Aspect Ratio (typical) where X=Aspect Ratio and Y=Acceptance Limit ..... 191

Figure 9-18: Example of interpolating for thickness..... 191

Figure 9-19: Interpolation Graph for Thickness (typical) Where X=Thickness and Y=Acceptance Limit ..... 192

Table 10-1: Natural focal spot sizes and near field for optimized 10 MHz, 64 elements, linear array probe with aperture 150 mm<sup>2</sup> ..... 195

Table 10-2: Specifications summary for the probes: central frequency, aperture and near field at -6dB ..... 196

Figure 10-1: Beam visualization at selected depth: (a) normal beam; (b) angle beam ..... 196

Table 10-3: Beam sizes of 10 MHz, 64 elements, linear array probe at depth 25mm: (a) Longitudinal Wave, no Wedge; (b) Shear Wave, Rexolite Wedge ..... 197

Figure 10-2: 10 MHz shear wave beam interactions–PAUT (left) and FMC/TFM T-T (right): (a) cluster of six SDHs; (b) notch ..... 198

Table 10-4: Vessels material and process parameters ..... 199

Figure 10-3: Calibrations: (a) normal beam (L-wave)–flexible wedge setup and L-L distance calibration imaging without TCG; (b) angle beam (S/T-wave)–flexible wedge setup and T-T distance calibration imaging without TCG; (c) angle beam (S/T-wave)–solid wedge setup, FMC/TFM T-T and PAUT SW distance calibration imaging with TCG. .... 200

Figure 10-4: Amplitude fidelity: (a) setup and pseudo A-scans; (b) T-T path/mode RoI; (c) failed T-T with RoI 30x25mm (width x height); (d) passed T-T with RoI 25x25mm (width x height)..... 201

Table 10-5: Pixel Size and Resolution/Wavelength Ratio for selected RoI..... 203

Figure 10-5: Scanning plans and typical C-, B-, D- views..... 203

Figure 10-6: FMC/TFM 3D imaging of carbon steel bar with machined flaws..... 204

Figure 10-7: Example of micro-machined clustered flaws: (a) picture; (b) skew 90 TFM imaging; (c) skew 270 TFM imaging ..... 205

Table 10-6: Clusters and SDHs height measurements using 10 MHz T-T path/mode..... 206

Table 10-7: SDHs vertical separation measurements using 10 MHz T-T path/mode..... 207

Figure 10-8: FMC/TFM LL imaging: (a) 15MHz imaging of non-damage block–pseudo A scan (top left), single plane B-scan (top right), single plane D-scan (bottom); (b) 10MHz projected C-scan of damage block; (c) 7.5MHz projected C-scan of damage block; (d) 5MHz projected C-scan of damage block; (e) 10MHz split screen imaging of selected indication: projected C-scan (left top), single plane B-scan (top right), single plane D-scan (bottom right), pseudo A-scan (bottom left)..... 208

Figure 10-9: Optical microscopy and SEM imaging of accelerated HTHA damage: (a) ~100X; as-polished; fissures forming relatively large micro crack; (b) ~100X; as-polished; fissures forming small micro crack; (c) ~5000X; Nital Etchant; SEM photograph of damage feature showing grain boundary void formation and some early stages of coalescence of

voids in the periphery of the main feature; (d) ~5000X; Nital Etchant; SEM photograph of damage feature showing severe dissolution of grain boundaries and some early stage of single void formation. .... 210

Figure 10-10: Setup for fully automated PAUT and FMC/TFM: (a) depentanizer reboiler channel; (b) zinc oxide drum ..... 212

Figure 10-11: 10 MHz T-T FMC/TFM and PAUT techniques imaging of HTHA weld damage: (a) linear probe C-scan and identification of the indications; (b) linear probe split screen views of indication #2; (c) indication of potential HTHA damage detected in the breaking areas using matrix probe and S-scan at skew-10° ..... 213

Figure 10-12: Weld damage validation using optical metallography and SEM: (a) root cracking (~20X, Nital etched); (b) stepwise macro cracking (~40X, Nital etched); (c) blisters (~40X, Nital etched); (d) voids along grain boundaries (~2,000X, Nital etched-left; ~20,000X, Nital etched-right); (e) stress-related micro cracking (~1,000X, Nital etched). .... 214

Figure 10-13: Imaging of Indication #10.1a.1 and #10.1a.2: (a) projected PAUT straight beam C-Scans comparison; (b) PAUT straight beam and FMC/TFM.ATFM LL B-Scans comparison; (c) comparison of PAUT S-Scans and FMC/TFM T-T B-scans using shear wave techniques..... 216

Figure 10-14: Metallographic and CT Images for Indications 10.1a.1 and 10.1a.2: (a) cutting plan; (b) x10, Indications 10.1a.1 and 10.1a.2; (c) Magnification x50, close up view of Indication 10.1a.1; (d) x50, close up view of Indication 10.1a.2; (e) CT images of Indication 10.1a.2 from 2 to 10mm below the polished surface of the mount. .... 218

Table 10-8: Height and width measurements of Indication#10.1a.1 ..... 220

Figure 10-15: Drum south section FMC/TFM imaging and HTHA validation: (a) localized and through wall distribution; (b) base material coupon cutting plan with C-scan overlay; (c) 3D imaging of blister-like damage; (d) optical metallography of linking voids merging into blisters, ~80X; As-Polished; (e) SEM validation of early stage HTHA volumetric damage, ~5,000X; Nital etched..... 221

Figure 10-16: Drum north section FMC/TFM imaging and HTHA validation: (a) raster C-scan imaging of possible HTHA damage–localized and through wall distribution; (b) visual validation of typical blister bulging; (c) line scan imaging of possible blistering with sharp crack-like edges; (d) optical metallography of blistering with sharp crack-like edges, ~50X, As-Polished; (e) SEM of non-metallic inclusions and evidence of early stage HTHA damage of void formation and voids coalescence, ~5000X, Nital etched. . 224

Figure 10-17: Primary Heat Transport piping arrangement between the steam generators and the fuel channels..... 227

Figure 10-18: Example showing the typical congestion of the feeder pipes..... 227

Figure 10-19: Example of FAC adjacent to the downstream weld toe..... 228

Figure 10-20: Inspection regions for welded fitting feeder configurations..... 230

Figure 10-21: Platform Operator clad in PPE at the Reactor Face work location. The radiation shielding canopy is absent in this view. .... 231

Figure 10-22: A view of the reactor face work platform with a shield canopy installed ..... 231

Table 10-9: Training Requirements..... 232

Figure 10-23: (right) Instrument cart with MicroPulse and Vault Interface Module (manipulator and peripheral electronics module), (left) couplant reservoir and calibration stand. .... 233

Figure 10-24: Manipulator for 2 1/2 inch NPS fittings installed on a mock-up..... 233

Figure 10-25: Manipulator for 2 inch NPS fittings ..... 233

Figure 10-26: Transducer for both 2 and 2 1/2 NPS sized manipulators. The transducer fires tangentially to the inspection surface with the sound redirected via a mirror. .... 233

Figure 10-27: Typical screen presentation of the developed software ..... 234

Figure 10-28: Example of the custom calibration block ..... 234

Figure 10-29: Manipulator arms..... 235

Figure 10-30: Example of a typical inspection record ..... 237

Figure 10-31: Example of a typical inspection record (cont.) ..... 238

Figure 10-32: TFM image of the Outside Diameter (OD) surface..... 238

Figure 10-33: Image showing the trace outline to define the OD surface..... 239

Figure 10-34: The TFM image of the interior ..... 239

Figure 10-35: Plotting of the ID interface ..... 240

Figure 10-36: Evaluation revealing the minimum thickness..... 240

Figure 10-37: Plotting of the ID and OD interface in a 3D model..... 240

Figure 10-38: Minor inclusion from fabrication welding..... 242

Figure 10-39: Image(s) result in an accurate visualization of the component..... 242

Figure 10-40: Section of an ex-service feeder demonstrating step erosion at the weld root. Flow is right to left in this image. .... 242

Figure 10-41: Example of the MIT result for a case where both the exterior and interior surfaces are independently and rapidly changing in profile. The hub is on the right, weld center and intrados of the fitting is on the left of the image..... 243

Figure 10-42: 3D image of a fitting-to-fitting weld color coded for thickness. Note the areas in black are outside the range of color coding for thickness. .... 244

Figure 10-43: 3D image of a 2 1/2 inch fitting to fitting weld color coded for thickness..... 244

Figure 10-44: Color-coded 3D representation of a 2 inch feeder fitting to fitting joint..... 244

Figure 10-45: Rotation of the 3D model ..... 244

Figure 10-46: Grey scale 3D model vs an actual photo of the component..... 245

Figure 10-47: OD imaged profiles vs the actual component..... 246

Figure 10-48: Illustration of a conventional SENB test specimen geometry ..... 248

Figure 10-49: Fatigue test setup on a servo-hydraulic test machine using an MTS clip gage ..... 248

Figure 10-50: The phased array ultrasonic technique setup to monitor the notch..... 249

Table 10-10: Periodic Crack Measurement Values Using Various Measurement Techniques..... 250

Figure 10-51: TFM images (left – T-T Mode, right – TT-T Mode), Number of Cycles = 0 ..... 250

Figure 10-52: PAUT image (Sectorial Scan), Number of Cycles = 0 ..... 251

Figure 10-53: TFM images (left–T-T Mode, right–TT-T Mode), Number of Cycles = 44914 ..... 251

Figure 10-54: PAUT image (Sectorial Scan), Number of Cycles = 44914..... 251

Figure 10-55: TFM images (left–T-T Mode, right–TT-T Mode), Number of Cycles = 66953 ..... 252

Figure 10-56: PAUT image (Sectorial Scan), Number of Cycles = 66953 ..... 252

Figure 10-57: TFM images (left–T-T Mode, right–TT-T Mode), Number of Cycles = 109833 ..... 252

Figure 10-58: PAUT image (Sectorial Scan), Number of Cycles = 109833 ..... 253

Figure 10-59: TFM images (left–T-T Mode, right–TT-T Mode), Number of Cycles = 129476 ..... 253

Figure 10-60: PAUT image (Sectorial Scan), Number of Cycles = 129476..... 253

Figure 10-61: TFM images (left–T-T Mode, right–TT-T Mode), Number of Cycles = 150378 ..... 254

Figure 10-62: PAUT image (Sectorial Scan), Number of Cycles = 150378..... 254

Figure 10-63: Graphical representation of fatigue crack growth measured using each technique..... 254

Table 10-11: Post-test Measurements ..... 255

Figure 10-64: Image of Sample 17279-4-13 used for detailed crack measurement..... 255

Table 10-12: Comparison between the four different crack measurement techniques in this study .. 256

Figure 10-65: SENB sample showing fatigue crack and corresponding FMC/TFM image of the crack ..... 256

Table 10-13: Example of Essential and Non-essential variables..... 257

Figure 10-66: Wedge Measurements..... 258

Figure 10-67: Considering variables ..... 259

Figure 10-68: Example of acoustic simulation for FMC/TFM scan planning. Image clearly shows the probe needs to be moved forward to achieve coverage of the weld root/I.D. HAZ, and in this way acoustic simulation proceeds much like the use of Ray Tracing..... 259

Figure 10-69: LOF and the response from differing image paths. From Left to right 2T Direct, 4T indirect, and Time Extended 2T ..... 260

Figure 10-70: Example of the Influence an incorrect thickness parameter has on the signal response of an I.D notch..... 261

Figure 10-71: Example of the influence an incorrect velocity parameter has on signal response. 5Mhz, n=64, P=0.6mm, T-T direct,  $\lambda/7$ , SDH @ 0.8 in. deep ..... 261

Table 10-14: General example of scan speed vs grid density for standard TFM. 5Mhz x 32-element probe. Changes to parameters such as PRF, algorithms and many others will affect results..... 262

Figure 10-72: A clear change is seen from  $\lambda/2$  to  $\lambda/5$ , but less from  $\lambda/5$  to  $\lambda/7$ . 1/64th SDH, 5Mhz, n=64, p= 0.6 mm, L-L image path, Envelope on, 1.57 in. index x 2.26 in. depth TFM frame..... 262

Figure 10-73: Image path verification on through wall slot in the ASME BPVC Section V calibration block. Satisfying the ASME requirements may require multiple image paths. .... 263

Figure 10-74: Examples of encoded scanning and data collection techniques..... 264

Figure 10-75: Example of data drop-out ..... 264

Figure 10-76: Example of typical scan layout..... 265

Figure 10-77: Example of Artifacts..... 265

Figure 10-78: Data View Schematic ..... 266

Figure 10-79: Measurement of Signal width. Note: Synthetic A-scans are produced from plotting the summed amplitudes in the image axis selected. Therefore, higher grid resolutions will produce higher resolution synthetic A-scans..... 267

Figure 10-80: Example of Rise and Fall..... 268

Table 10-15: Key to flaws shown in Figure 10-81 and Figure 10-82 ..... 269

Figure 10-81: Weld scanned from both sides with 0.600 in. (15.2 mm) index position ..... 270

Figure 10-82: Weld scanned from both sides with 1.800 in. (46 mm) index position ..... 270

Figure 10-83: End view response from 0.5in. (13 mm) Single V, Sidewall LOF–270 side ..... 271

Figure 10-84: End view response from 0.5in. (13 mm) Single V, Porosity–Center Line ..... 271

Figure 10-85: End view response from 0.5in. (13 mm) Single V, Root Crack–90 side..... 272

Figure 10-86: End view response from 0.5in. (13 mm) Single V, OD HAZ crack–270 side ..... 272

Figure 10-87: End view response from 0.5in (13 mm) Single V, Lack of Penetration–Center Line. 273

Figure 10-88: End view response from 0.5in. (13 mm) Single V, Slag–Center Line ..... 273

Figure 10-89: End view response from 1 in. (25 mm) Double V, LOF–Bottom Bevel, 270 side..... 274

Figure 10-90: End view response from 1 in. (25 mm) Double V, Center Line Crack ..... 274

Figure A-1: TFM T-T mode of 30% ID notches ..... 279

Figure A-2: TFM T-T mode of 30% ID notches ..... 280

Figure A-3: TFM T-T mode of 30% ID notches ..... 281

Figure A-4: TFM T-T mode of 30% ID notches ..... 282

Figure A-5: TFM T-T mode of 30% OD notches, spherical. Sound is sent towards the notch acute angles..... 283

Figure A-6: TFM T-T mode of 30% OD notches, spherical. Sound is sent towards the notch obtuse angles..... 284

Figure A-7: TFM T-T mode of 30% OD notches ..... 285

Figure A-8: TFM T-T mode of 30% OD notches ..... 286

Figure A-9: TFM TT-T, TT-TT & TT-TTT modes of 30% ID notches ..... 287

Figure A-10: TFM TT-T, TT-TT & TT-TTT modes of 30% ID notches, spherical. Sound is sent towards the notch obtuse angles. .... 288

Figure A-11: TFM TT-T, TT-TT & TT-TTT modes of 30% ID notches ..... 289

Figure A-12: TFM TT-T, TT-TT & TT-TTT modes of 30% ID notches ..... 290

Figure A-13: TFM TT-T, TT-TT & TT-TTT modes of 30% OD notches..... 291

Figure A-14: TFM TT-T, TT-TT & TT-TTT modes of 30% OD notches.....	292
Figure A-15: TFM TT-T, TT-TT & TT-TTT modes of 30% OD notches.....	293
Figure A-16: TFM TT-T, TT-TT & TT-TTT modes of 30% OD notches.....	294
Figure A-17: TFM T-T, TT-T, TT-TT & TT-TTT modes of 30% ID notches .....	295
Figure A-18: TFM T-T, TT-T, TT-TT & TT-TTT modes of 30% ID notches .....	296
Figure A-19: TFM T-T, TT-T, TT-TT & TT-TTT modes of 30% ID notches .....	297
Figure A-20: TFM T-T, TT-T, TT-TT & TT-TTT modes of 30% ID notches .....	298
Figure A-21: TFM T-T, TT-T, TT-TT & TT-TTT modes of 30% OD notches.....	299
Figure A-22: TFM T-T, TT-T, TT-TT & TT-TTT modes of 30% OD notches.....	300
Figure A-23: TFM T-T, TT-T, TT-TT & TT-TTT modes of 30% OD notches.....	301
Figure A-24: TFM T-T, TT-T, TT-TT & TT-TTT modes of 30% OD notches.....	302
Figure B-1: Instrumentation–Olympus X3.....	303
Figure B-2: Ultrasonic Setup.....	303
Figure B-3: Weld Configuration .....	304
Figure B-4: Display Configuration.....	304
Figure B-5: Sample U587.....	305
Figure B-6: Sample U587–Flaw 1, T-T–Depth=4.66 mm/Height=4.66 mm .....	305
Figure B-7: Sample U587–Flaw 2, TT-T–Depth=25.4 mm/Height=4.75 mm.....	306
Figure B-8: Sample U587–Flaw 2, T-T–Depth=25.4 mm/Height=4.75 mm .....	307
Figure B-9: Sample U587–Flaw 3, TT-TT–Depth=8.60 mm/Height=4.00 mm .....	308
Figure B-10: Sample U585.....	309
Figure B-11: Sample U585–Flaw 1, TT-T–Depth=25.4 mm/Height=5.36 mm.....	309
Figure B-12: Sample U585–Flaw 1, T-T–Depth=25.4 mm/Height=4.86 mm .....	310
Figure B-13: Sample U585–Flaw 2, T-T–Depth=25.4 mm/Height=3.13 mm .....	311
Figure B-14: Sample U585–Flaw 2, TT-TT–Depth=25.4 mm/Height=4.54 mm .....	312
Figure B-15: Sample U585–Flaw 3, TT-TT–Depth=3.54 mm/Height=3.54 mm .....	313
Figure B-16: Sample UT1639 .....	314
Figure B-17: Sample UT1639–Flaw 1, TT-TT–Depth=2.45 mm/Height=2.45 mm.....	314
Figure B-18: Sample UT1639–Flaw 2, TT-TT–Depth=20.95 mm/Height=2.40 mm.....	315
Figure B-19: Sample UT1639–Flaw 3, TT-TT–Depth=25.4 mm/Height=3.41 mm.....	316
Figure B-20: Sample UT1632 .....	317
Figure B-21: Sample UT1632–Flaw 1, TT-TT–Depth=2.73 mm/Height=2.73 mm.....	317
Figure B-22: Sample UT1632–Flaw 2, TT-TT–Depth=25.4 mm/Height=4.11 mm.....	318
Figure B-23: Sample UT1632–Flaw 3, TT-TT–Depth=9.68 mm/Height=3.52 mm.....	319
Figure B-24: Sample UT6164 .....	320
Figure B-25: Sample UT6164–Flaw 15, TT-TT–Depth=4.39 mm/Height=2.68 mm .....	320
Figure B-26: Sample UT6164–Flaw 15, TT-T–Depth=4.95 mm/Height=3.64 mm.....	321
Figure B-27: Sample UT6164–Flaw 30, TT-TT–Depth=4.50 mm/Height=3.56 mm .....	322
Figure B-28: Sample UT6161 .....	323
Figure B-29: Sample UT6161–Flaw 37, TT-TT–Depth=5.53 mm/Height=2.48 mm.....	323
Figure B-30: Sample UT 6151 .....	324
Figure B-31: Sample UT 6151–Flaw 37, TT-TT–Depth=5.52 mm/Height=2.02 mm.....	324
Figure B-32: Sample UT 6151, Unreported flaw .....	325
Figure B-33: Sample UT6154 .....	326
Figure B-34: Sample UT6154–Flaw 15, TT-T–Depth=4.95 mm/Height=3.61 mm.....	326
Figure B-35: Sample UT6154–Flaw 15, TT-T–Depth=4.72 mm/Height=4.72 mm .....	327
Figure B-36: Sample UT6154–Flaw 30, TT-TT–Depth=5.02 mm/Height=5.02 mm .....	328
Figure B-37: Sample UT6159 .....	329
Figure B-38: Sample UT6159–Flaw 18, T-T–Depth=3.89 mm/Height=3.89 mm .....	329
Figure B-39: Sample UT6159–Flaw 19, T-T–Depth=15.0 mm/Height=3.29 mm .....	330
Figure B-40: Sample UT6159–Flaw 19, TT-TT–Depth=15.0 mm/Height = 4.76 mm .....	331

Figure B-41: Sample UT 1813-Flaw 1, TT-TT-Depth=3.55 mm/Height = 3.55 mm .....	332
Figure B-42: Sample UT 1813-Flaw 2, TFM-Depth=19.1 mm/Height = 3.03 mm .....	333
Figure B-43: Sample UT1814-Flaw 2, TFM-Depth=19.1 mm/Height = 2.83 mm .....	334
Table B-1: Sizing.....	335

## ACKNOWLEDGEMENTS

Upon the publication of the 2019 Edition of the ASME BPVC Section V, rules were established for Full Matrix Capture (FMC) in Article 4, Mandatory Appendix XI. This took an exceptional group of volunteers who came together and were able to dedicate time and establish processes which would allow us to finish an exceedingly challenging task in less than half the normal time.

Recognizing that we had provided a great service to industry for an emerging technology, we understood that to be truly successful, more was needed. It was obvious that there was strong interest for FMC. However, apprehension also took hold. Besides having a set of rules in the Code, a better understanding of the technology would further promote its use, and most importantly prevent a repeat of some of the mistakes of the past.

While some of us moved on after the publication of the Code rules, others remained, and soon, others would join us in the endeavor to bring this training manual to light. It cannot go without being said that only through the expertise of volunteers, and selfless sacrifice, being that of a great deal of time and dedication, would this work even be possible. The expense, let alone assembling this much talent, for the purpose of publishing a training manual such as this would otherwise have been impossible. Indeed, this was truly an exceptional group of individuals.

We also recognize that by writing this training manual, a precedent was set for ASME BPVC Section V. We would like to thank ASME for this opportunity, and hope that others will follow. Education is paramount.

### **The Authors:**

Paul Hayes (Chair) – Sinewave Solutions  
Emilie Peloquin (Vice Chair) – Evident Scientific  
Dr. James Barshinger – Sensor Networks Inc.  
Timothy Greisbach – Structural Integrity Associates (Ret.)  
Ray ten Grotenhuis – Ontario Power Generation  
William Lindo – Mistras  
Dr. Mark Lozev – BP (Ret.)  
Michael Monnette – Eddyfi Technologies  
Renato Nogueira – Sonatest  
Daniel Richard – Zetec  
Erica Schumacher – EXTENDE  
Oleg Volf – TWI  
Shane Walton – University of Ultrasonics  
Dr. Casper Wassink – Eddyfi Technologies

### **Contributing Authors:**

Adri van den Biggelaar – RTD  
Johann Catty - CETIM  
Dr. George Connolly – EPRI  
Jimmy Ellis – Jimmy Ellis LLC  
Dr. Lars Horchens – RTD  
Dr. Richard “Rick” Jacobs - PNNL  
Dr. Alain LeDuff – Evident Scientific  
Dr. Neils Portzgen – RTD  
Carlton R. M. Ramcharran – ASME

## FOREWORD

Established in 1880, ASME is a professional not-for-profit organization with more than 100,000 members promoting the art, science, and practice of mechanical and multidisciplinary engineering and allied sciences. ASME develops codes and standards that enhance public safety, and ASME provides lifelong learning and technical exchange opportunities benefiting the engineering and technology community. Visit [www.asme.org](http://www.asme.org) for more information.

ASME ST-LLC is a not-for-profit limited liability company, with ASME as the sole member, formed in 2004 to carry out work related to new and developing technologies. ASME ST-LLC's mission includes meeting the needs of industry and government by providing new standards-related products and services, which advance the application of emerging and newly commercialized science and technology and provides the research and technology development needed to establish and maintain the technical relevance of codes and standards. Visit <http://asmestllc.org/> for more information.



## 1 HISTORY

### 1.1 ASME History

ASME has been around for more than 140 years, starting with the first meeting in the spring of 1880 in New York. As ASME was born during the industrial revolution, the meeting was largely attended by prominent industrialists of the time. The intention was to provide a forum for discussion and collaboration to better serve the needs of engineers and designers. The history of ASME cannot be appreciated without mentioning some of the consequences from the industrial revolution, two of which are boiler explosions and the need for standardization. Safety and standardization are still the main vision and mission for ASME.

The industrial revolution was made possible by the application of steam power as an energy source. In fact, the advent of steam power quickly became the industrializing nations' dominant power source. For example, the use of steam power increased from just 5% to 80% of the total power in the United States over a 20-year span in the mid-1800's. Today, steam energy (i.e., steam-driven turbines) still supplies 80% of the world's electricity.

When water converts to steam it expands ~1600 times in volume, which can generate enormous pressures. The use of steam to drive machinery was discovered to be a vast improvement over existing water mills, windmills, and even beast-of-burden power. However, early boilers from this period commonly suffered from catastrophic failures (i.e., explosions), mainly due to poor materials, poor design, and poor maintenance.

The earliest boilers were made of small wrought iron plates that were riveted together, but other materials such as copper were also commonly used. Quality improved with the use of rolled steel plates, but construction consisted of gusseted or slip-joint designs with rivets (see Figure 1-1). Acetylene was not discovered until 1836, and “conventional welding,” as it is presently known, was not developed until 1881. Repairs made to boilers were left up to “best practice,” which meant there were no standards of methods or quality.

**Figure 1-1: Period Repair Work on a Riveted Seam**



Image Courtesy of Sinewave Solutions